Supplementary Appendix

This appendix has been provided by the authors to give readers additional information about their work.

Supplement to: Lisco A, Hsu AP, Dimitrova D, et al. Treatment of relapsing HPV diseases by restored function of natural killer cells. N Engl J Med 2021;385:921-9. DOI: 10.1056/NEJMoa2102715

Supplementary Materials:

1. **Supplementary Figures 1-17……..page 2**
2. **Supplementary Figures Legends……page 19**
3. **Supplementary Methods…….page 25**
4. **Supplementary Table……..page 34**
5. **Supplementary Methods References…….page 35**

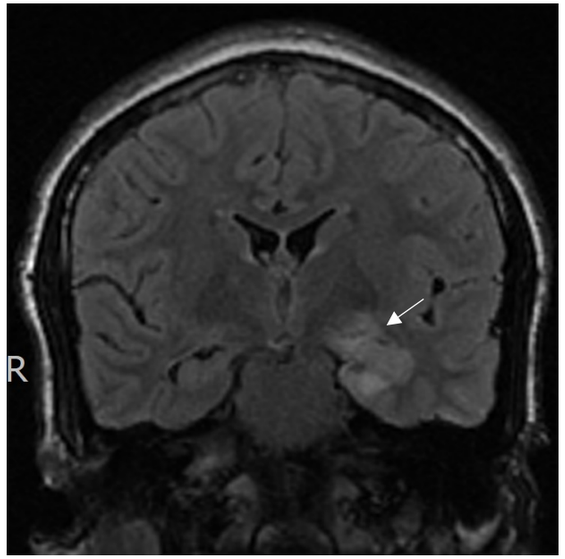

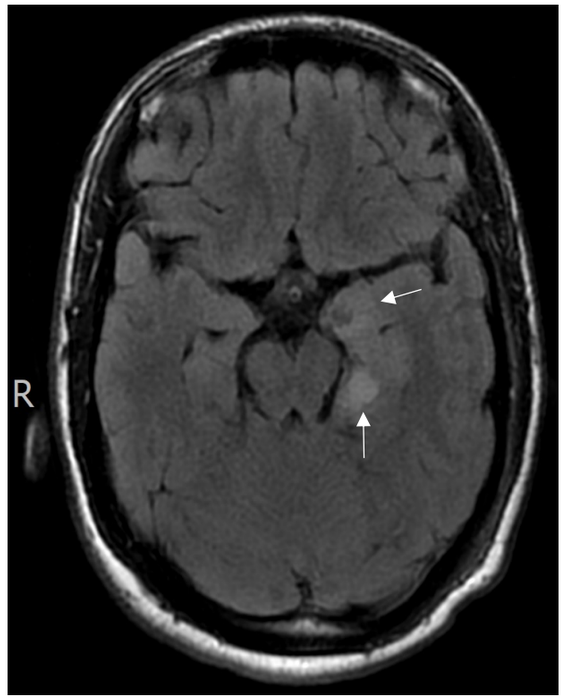

Supplemental Figure 1

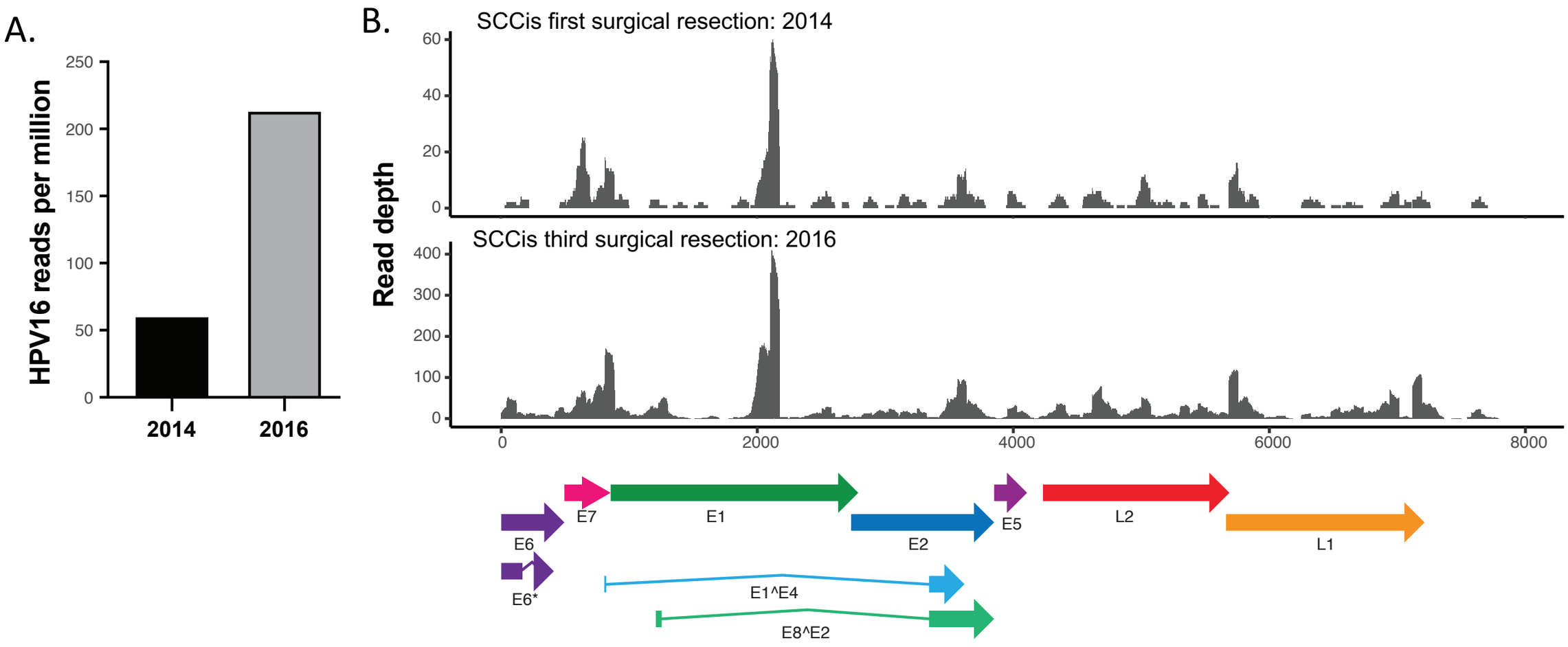

Supplemental Figure 2

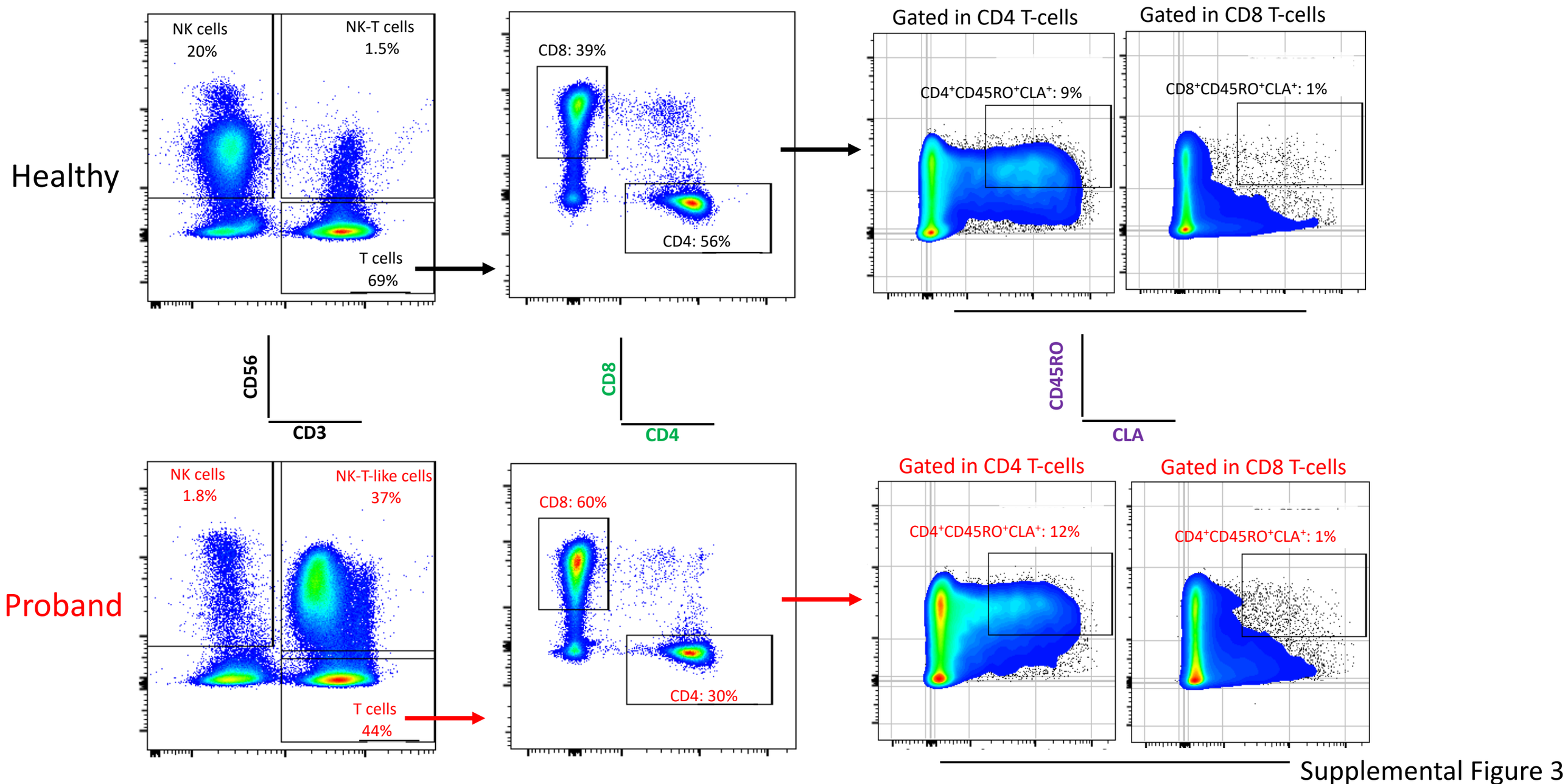

Supplemental Figure 3

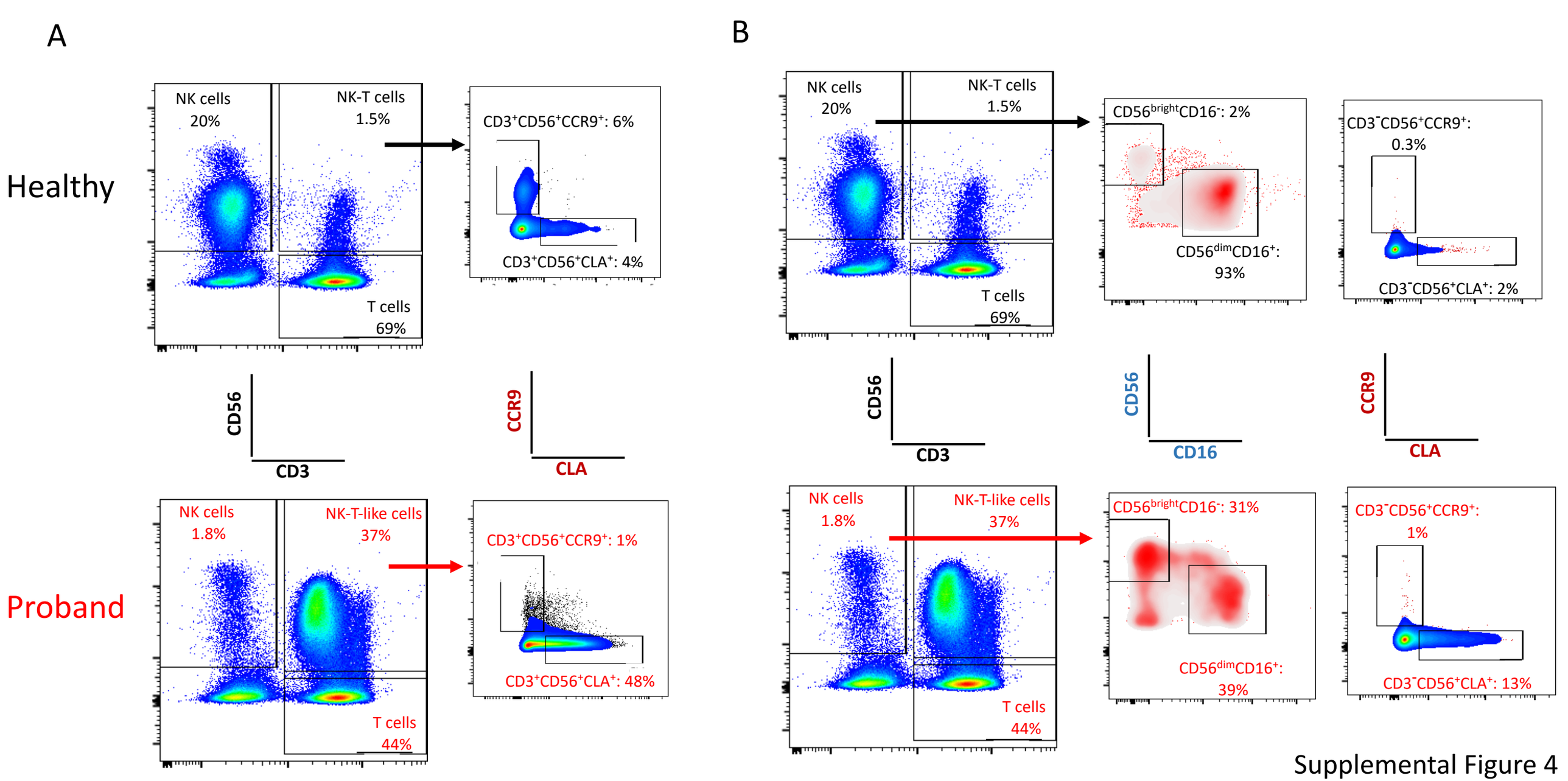

Supplemental Figure 4

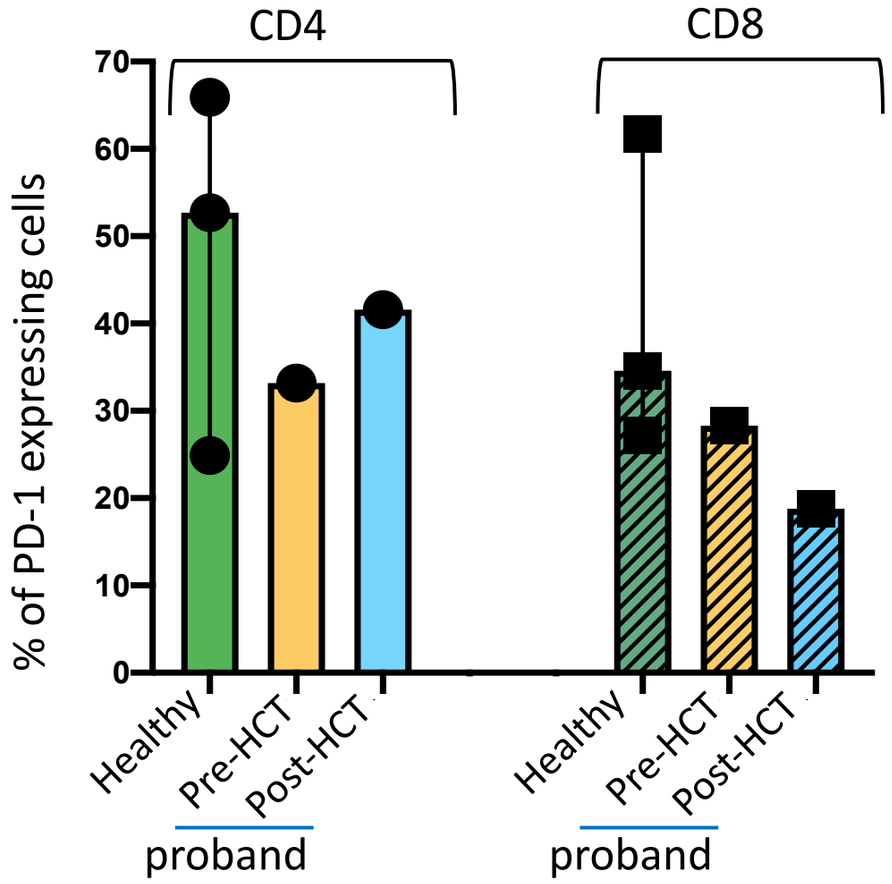

Supplemental Figure 5

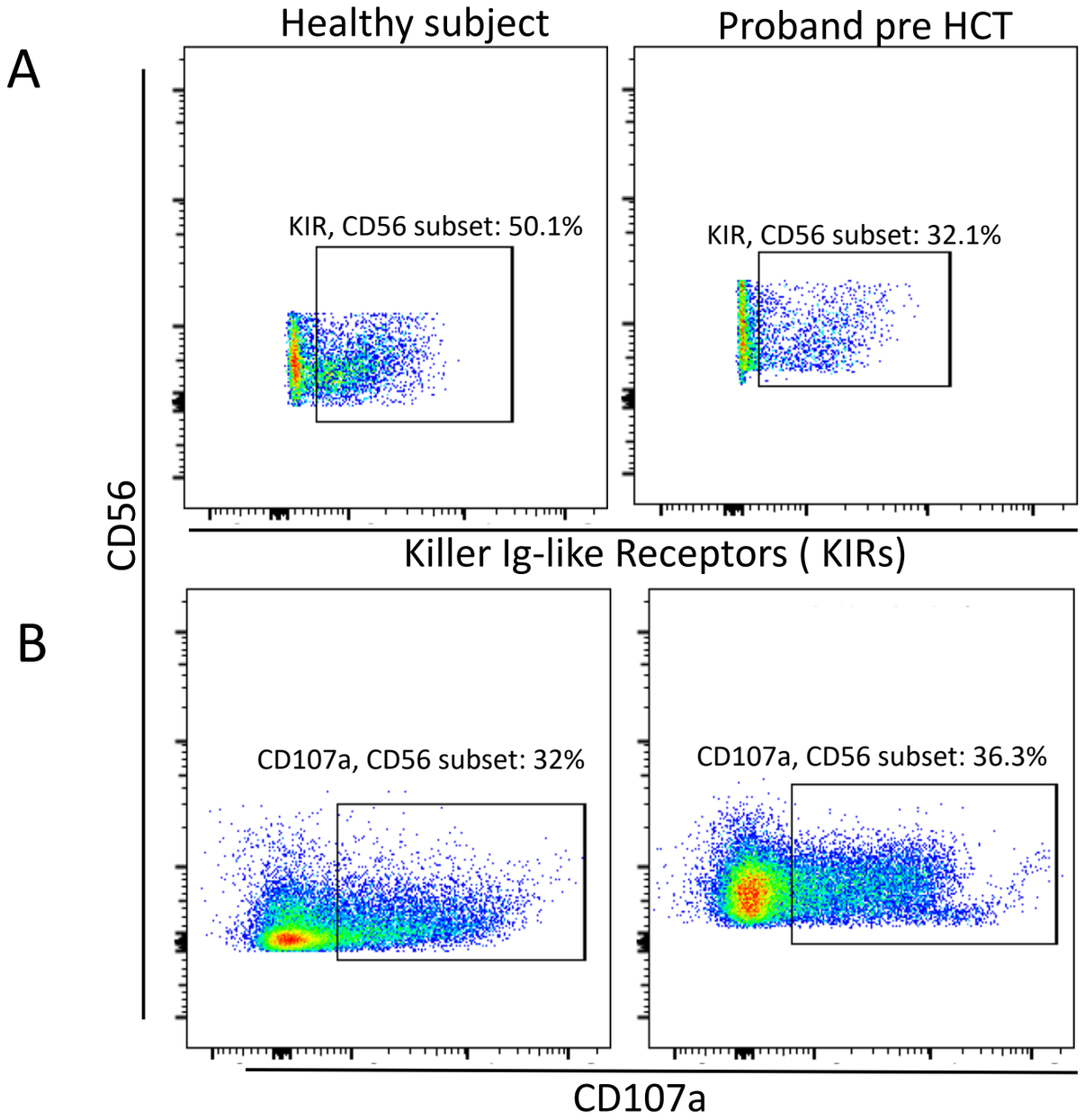

Supplemental Figure 6

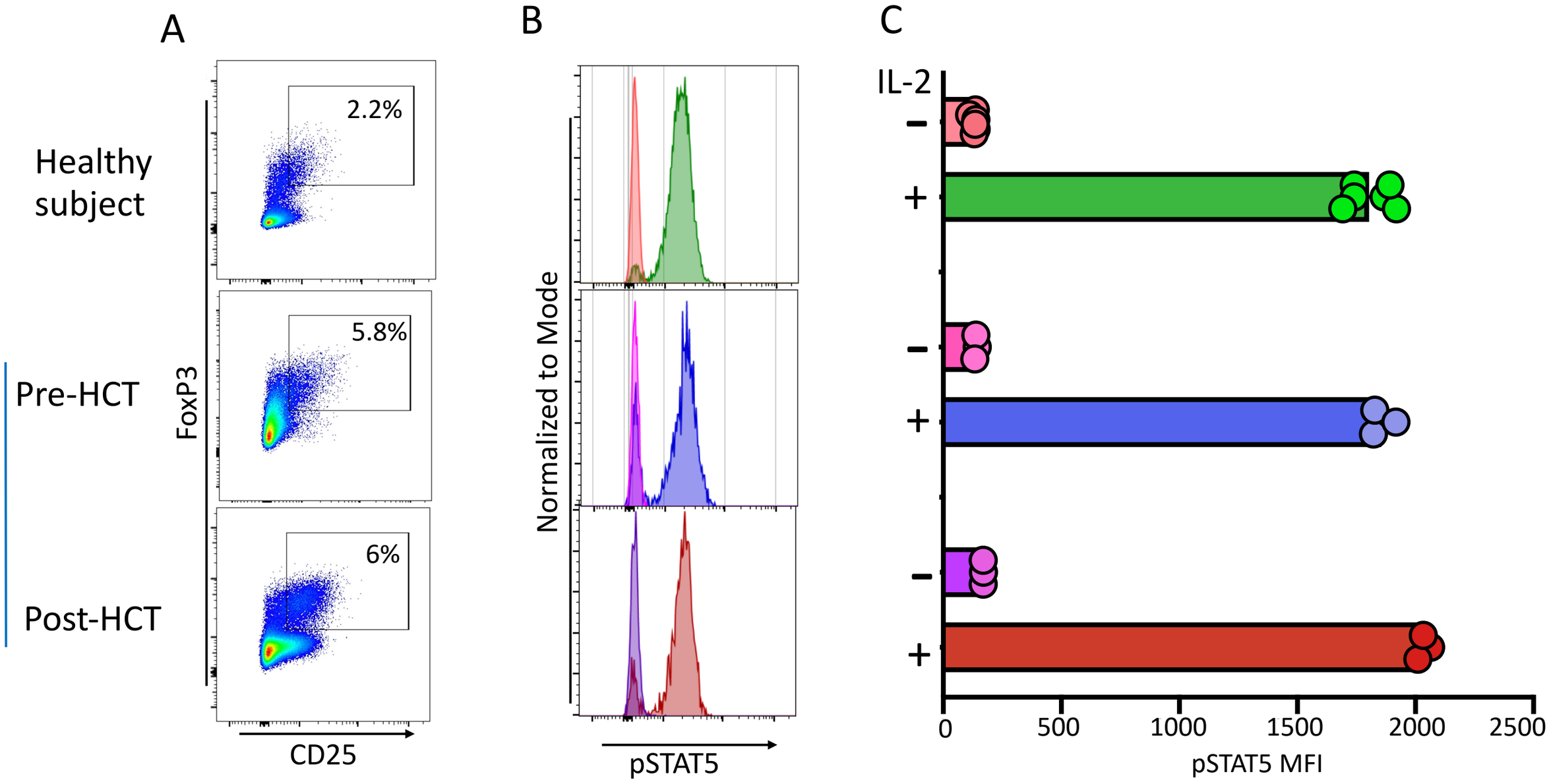

Supplemental Figure 7

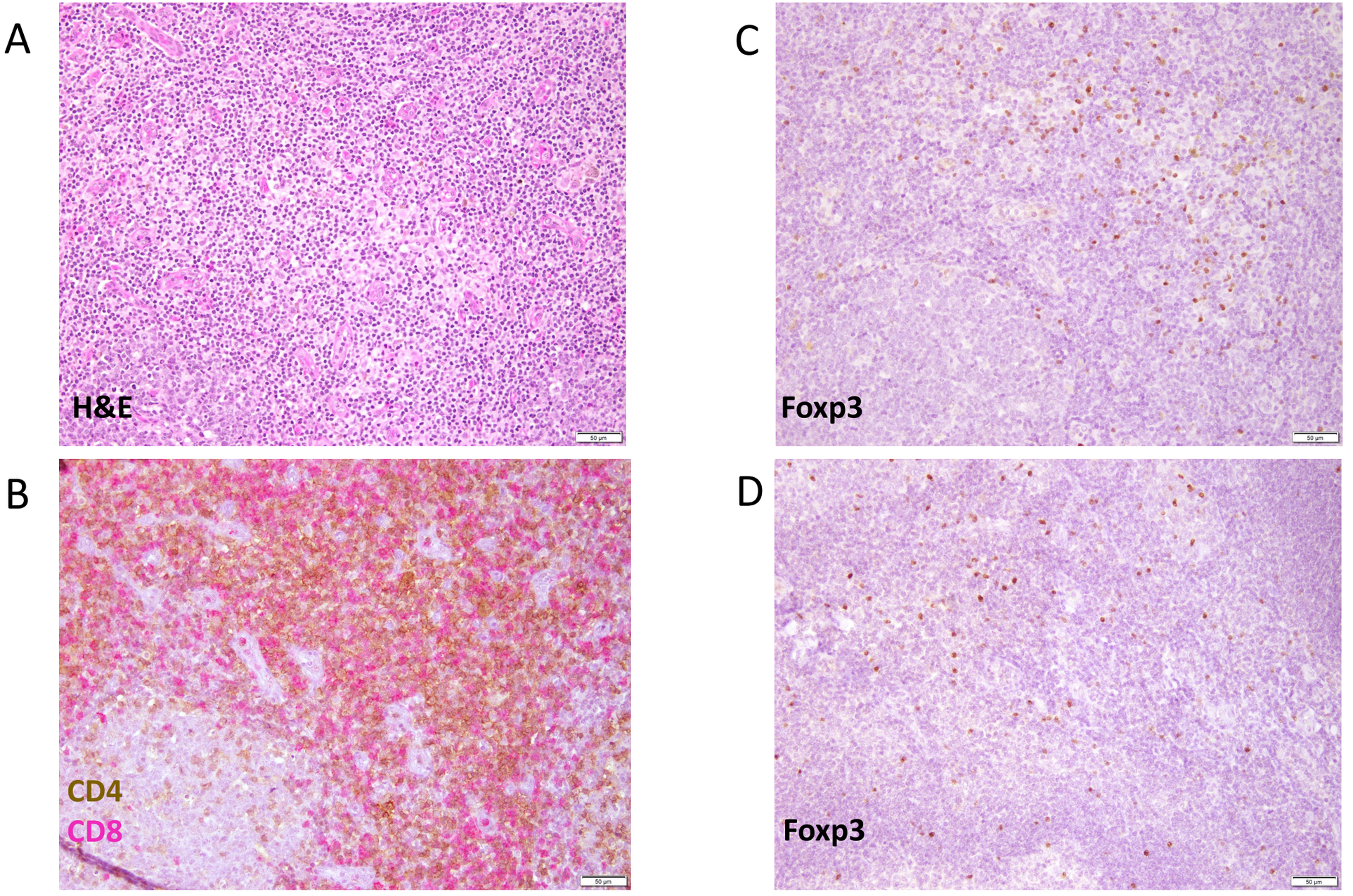

Supplemental Figure 8

A

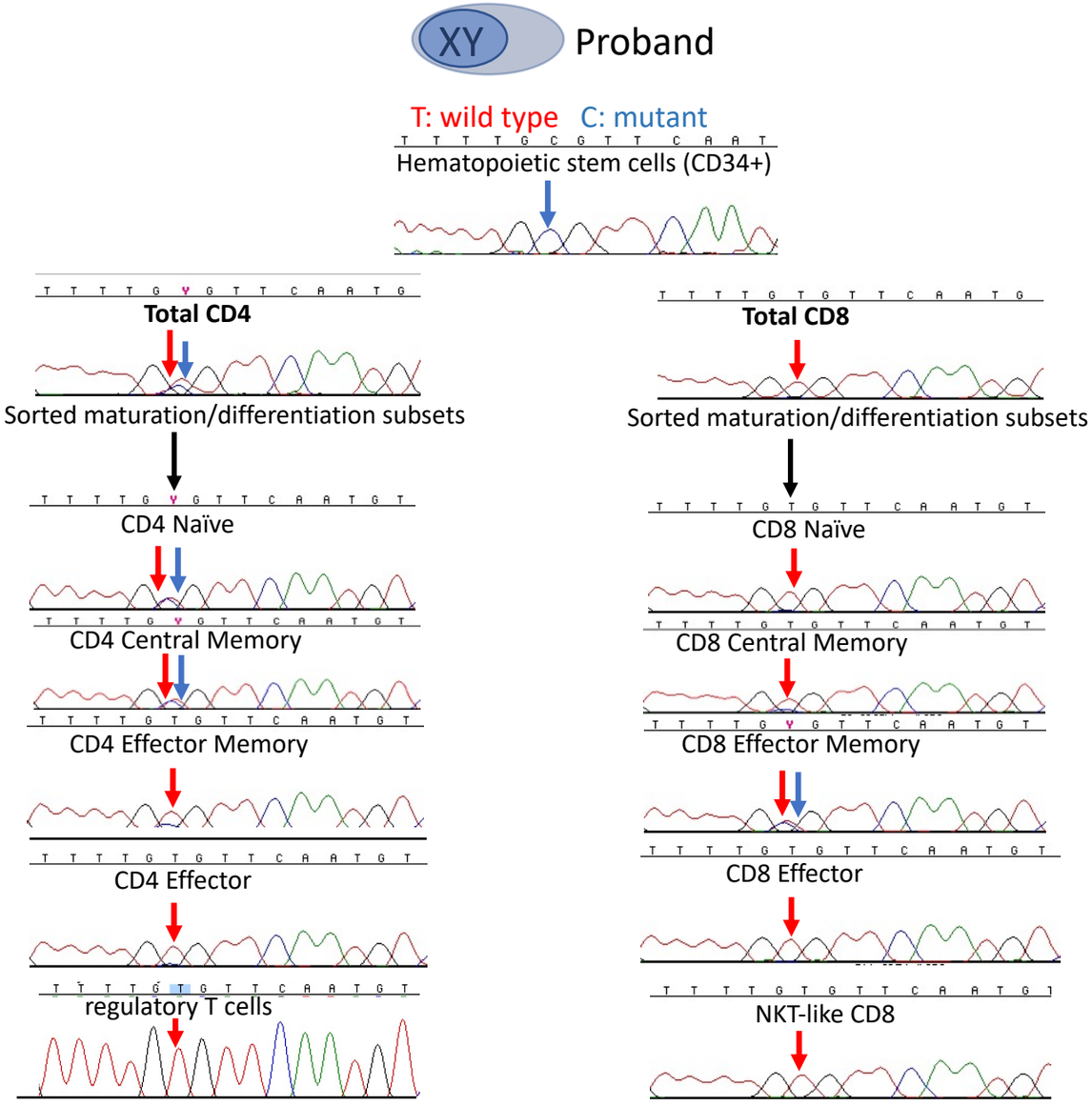

B

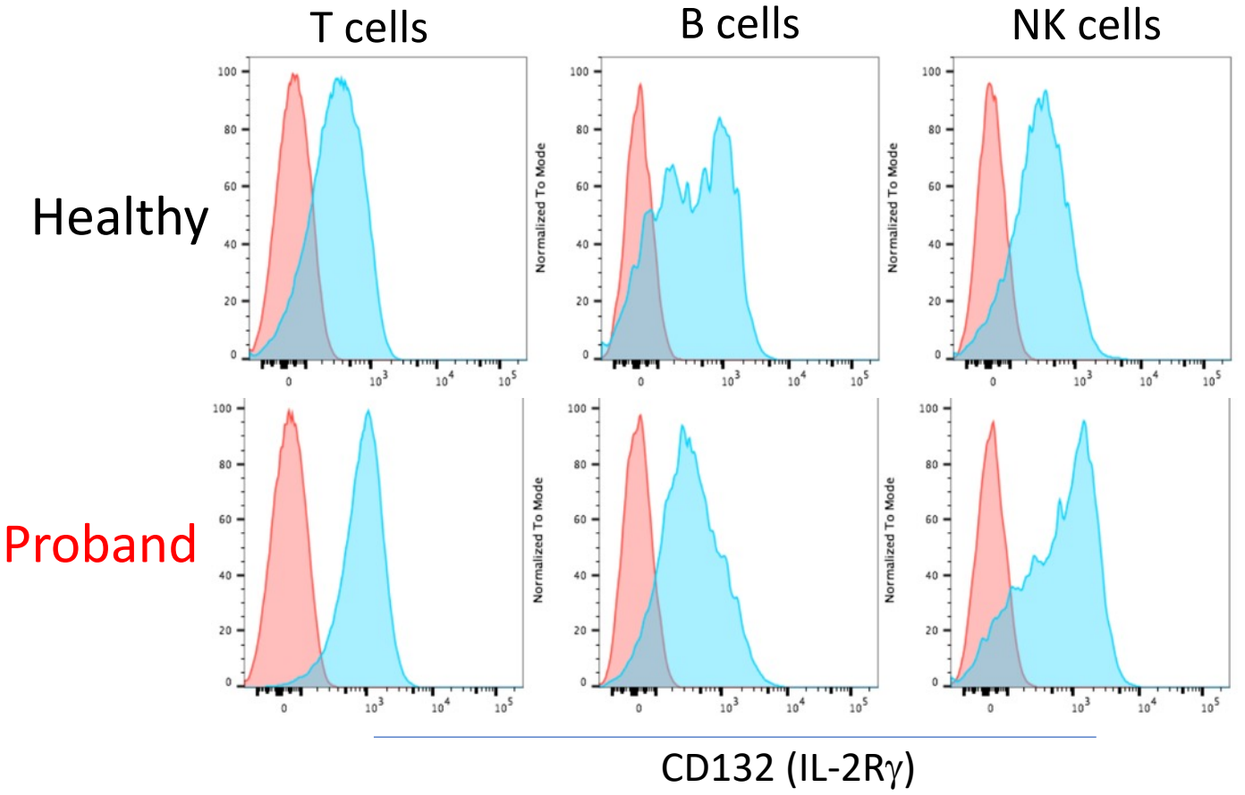

Supplemental Figure 9

A

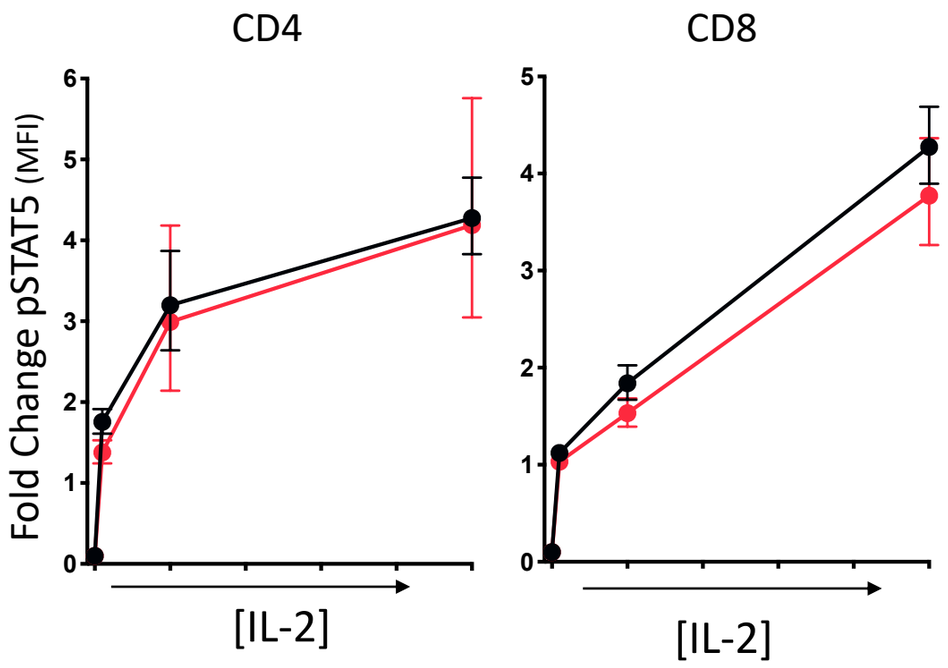

B

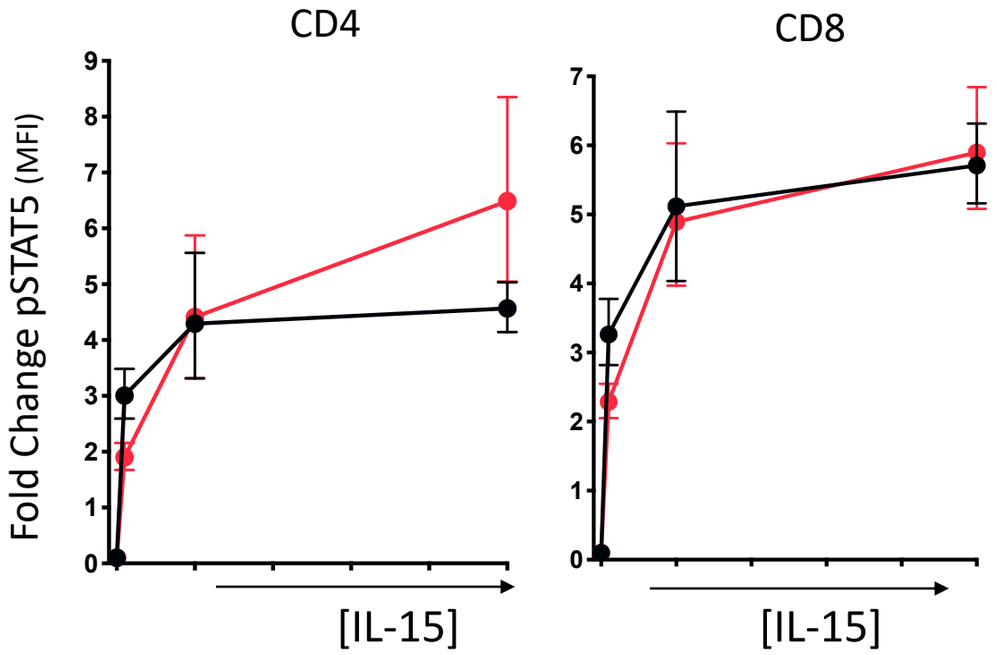

Healthy
Proband

Supplemental Figure 10

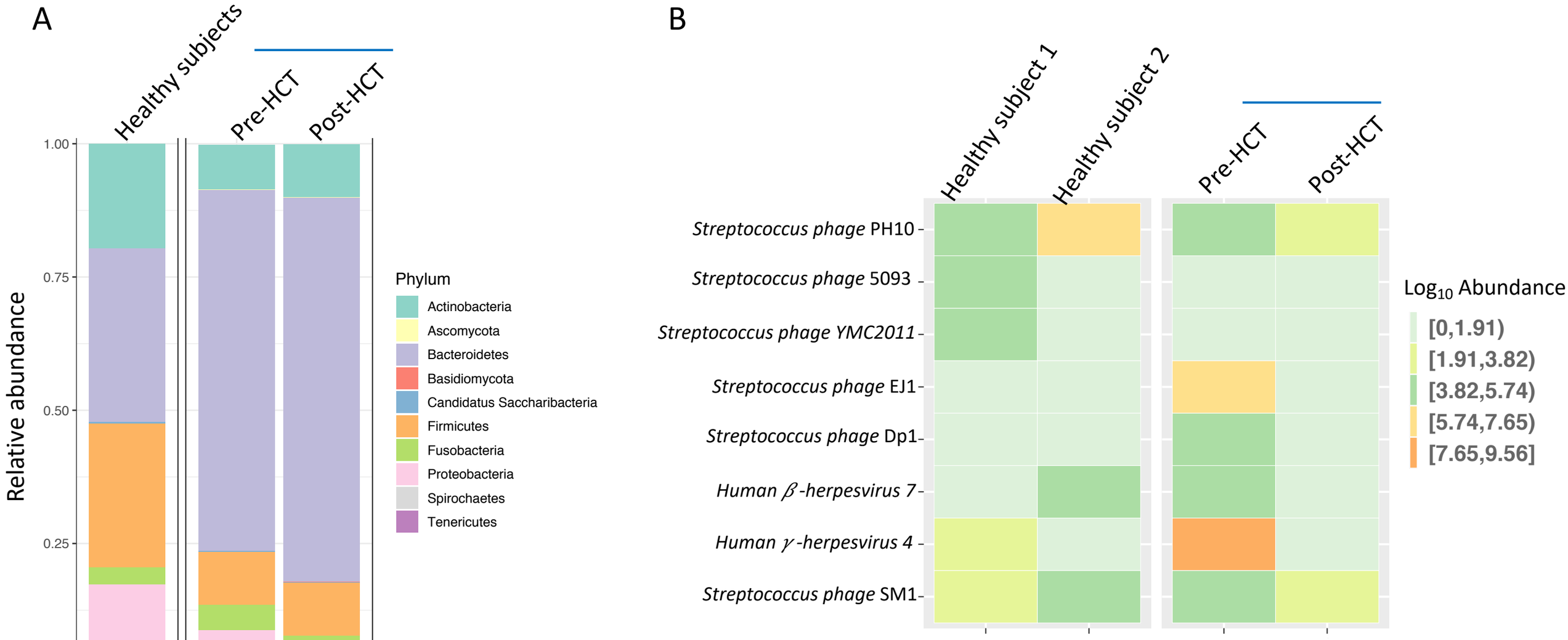

Supplemental Figure 11

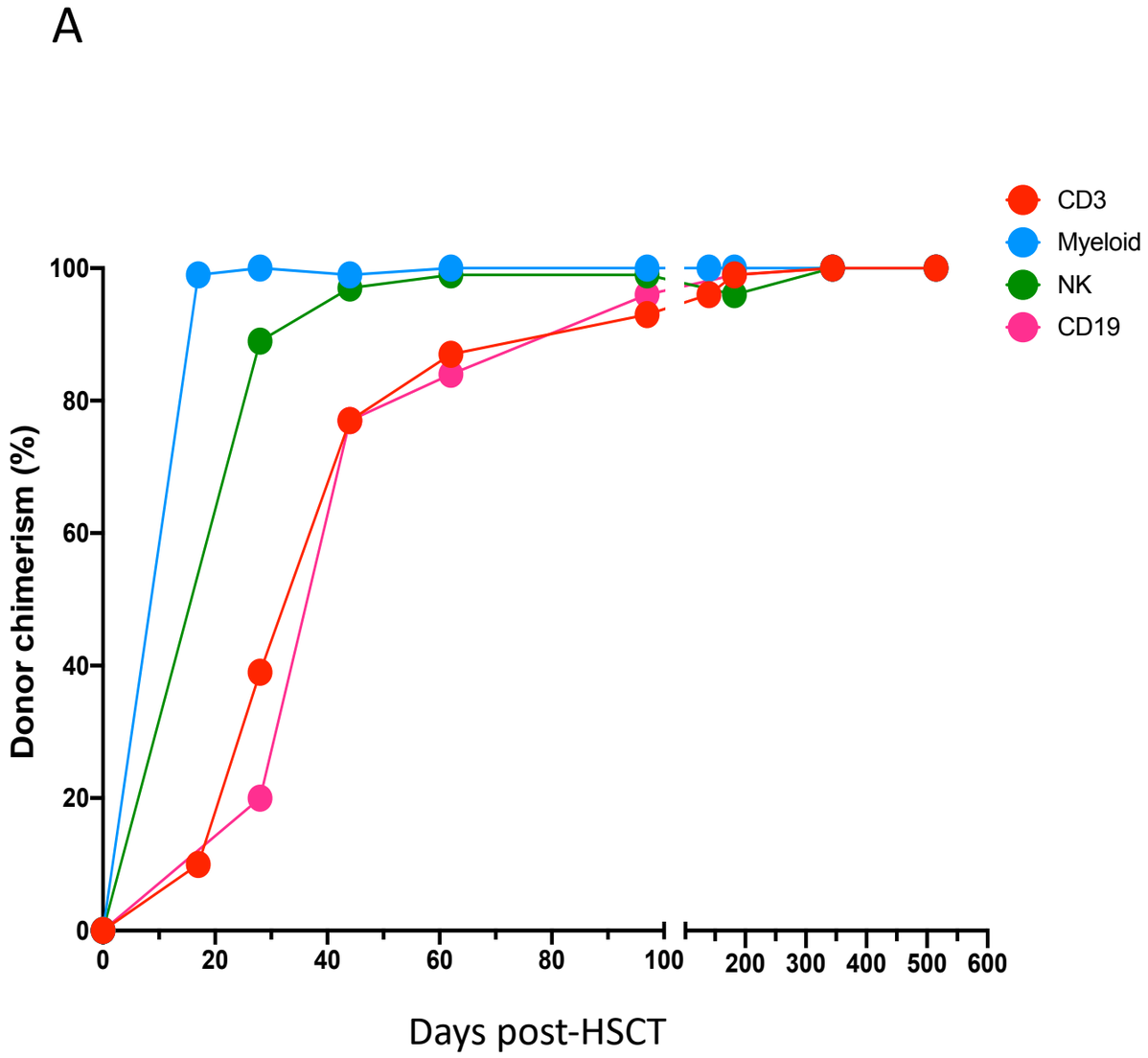

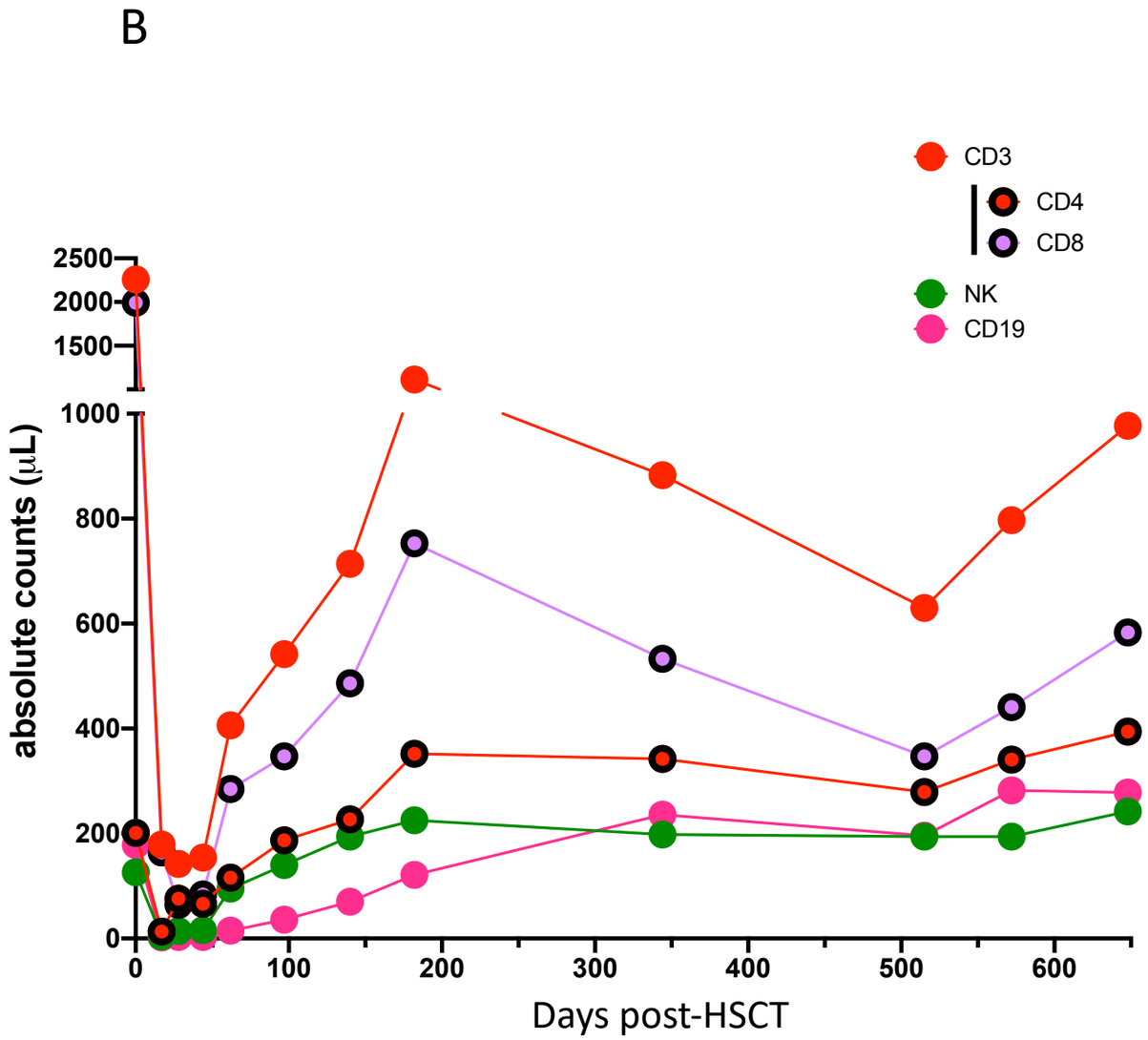

Supplemental Figure 12

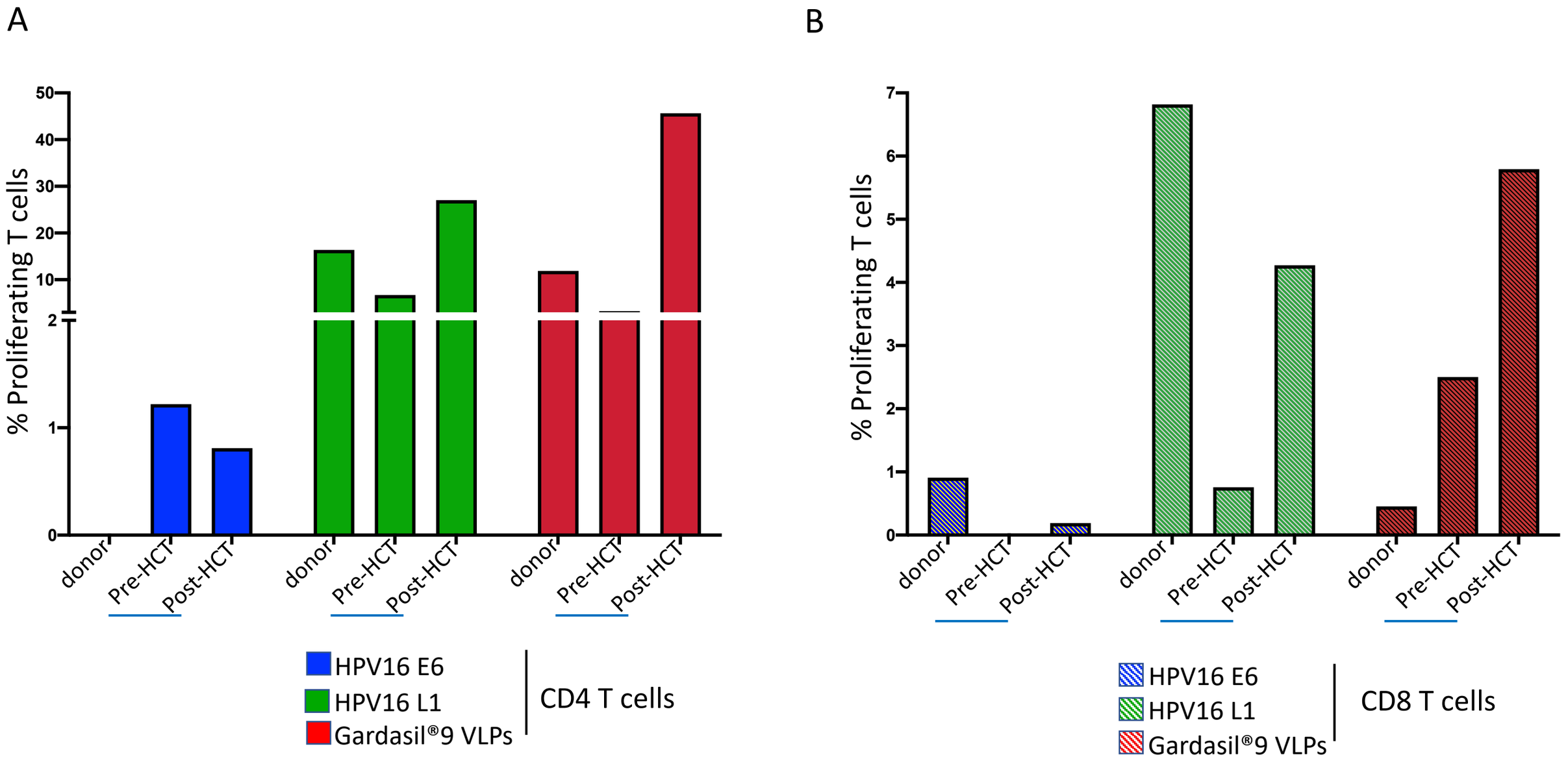

Supplemental Figure 13

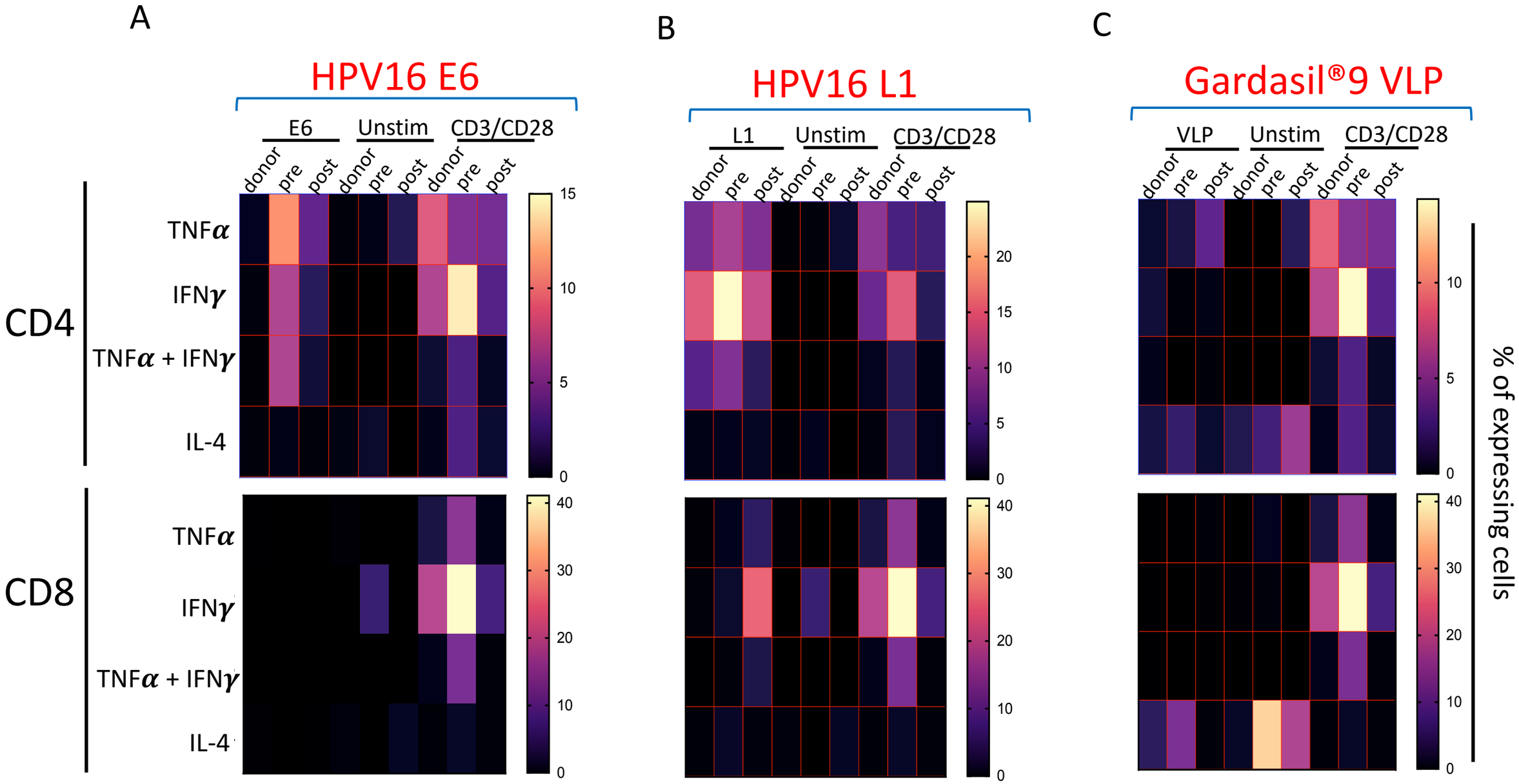

Supplemental Figure 14

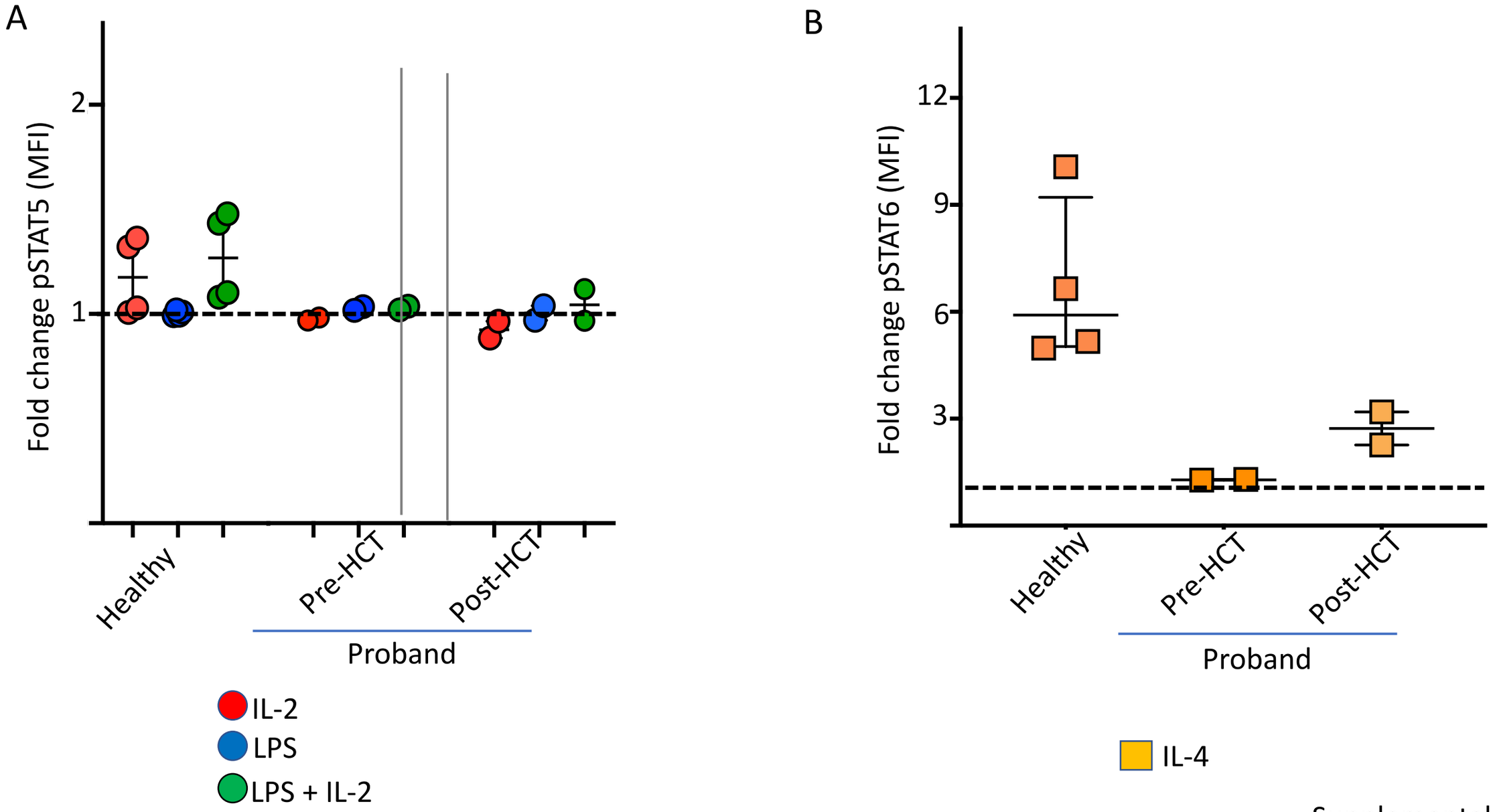

Supplemental Figure 15

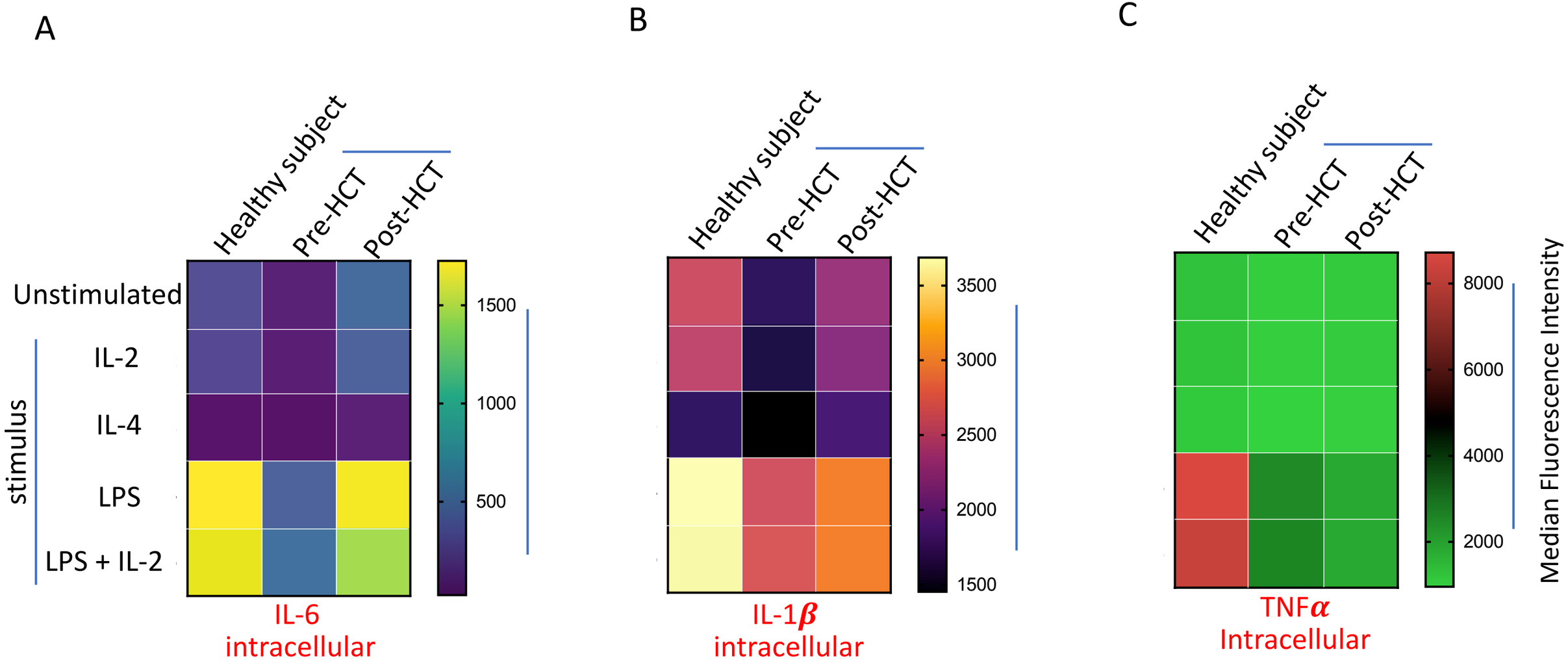

Supplemental Figure 16

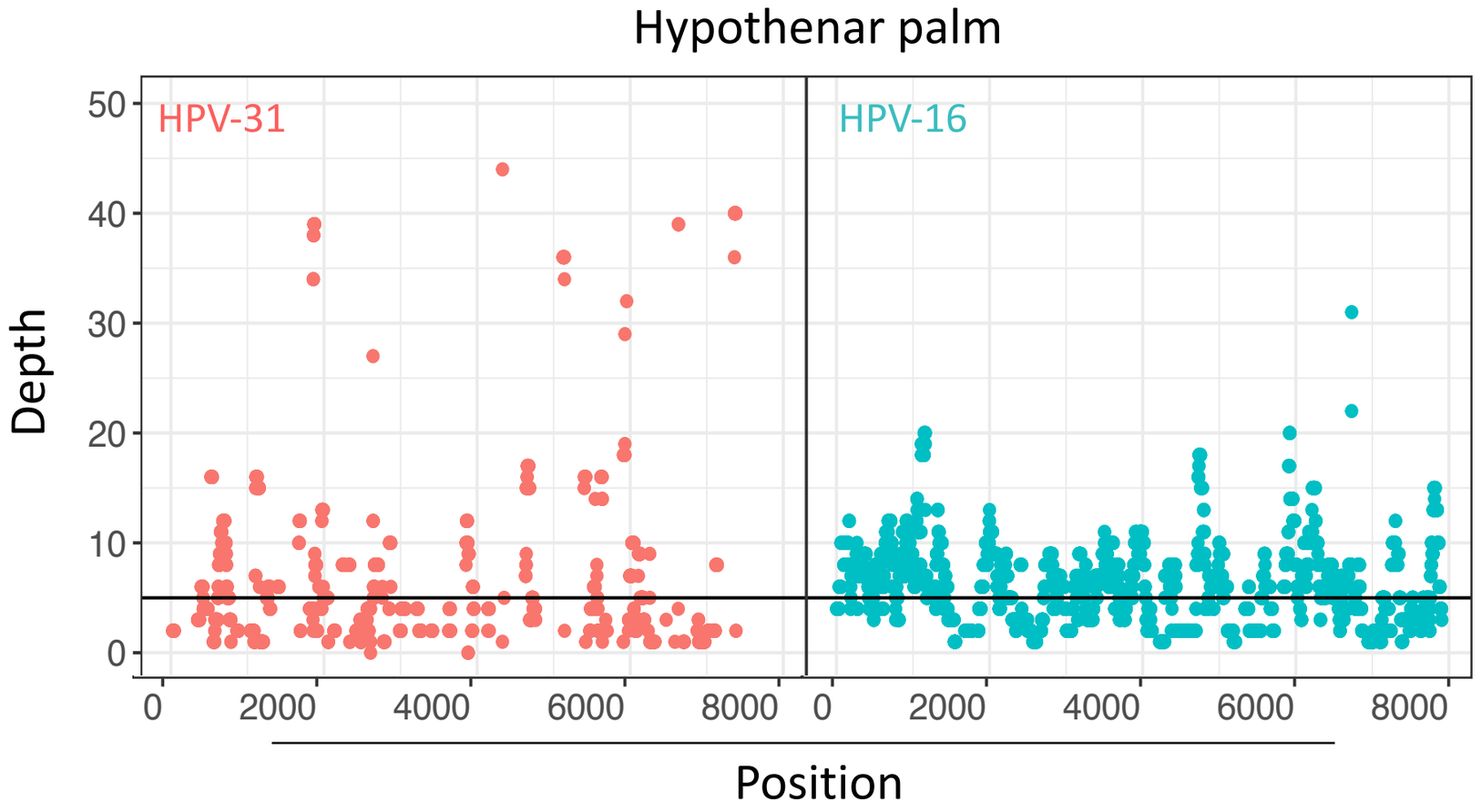

Supplemental Figure 17

2. Supplementary Figures Legends:

Supplementary Figure 1:

A, B: Magnetic resonance imaging of the brain: Coronal (**A**) and axial (**B**) FLAIR images showing increased signal intensity in the left medial temporal lobe (white arrows).

C, D: Flat warts (verruca plana) and scattered verruca vulgaris extending beyond the hairline on forehead and neck prior HCT. Note the linear pattern of neck verrucous lesions possibly suggestive of Koebner phenomenon in area of skin trauma (white arrow).

E, F: Complete resolution of verruca plana and verruca vulgaris in the forehead and posterior neck respectively 36 months and 24 months after HCT.

Supplementary Figure 2:

A. Number of HPV16 reads normalized per million human reads for each sample of paraffin embedded tissue derived from the surgical resection of the nasal squamous carcinoma *in situ* (SCCis) in 2014 and 2016.

B. RNA seq coverage plots of HPV16 from the 2014 and 2016 samples. The different HPV16 open reading frames are shown below.

Note that the RNAseq molecular analysis is consistent with an HPV-16 driven nasal SCCis.

Supplementary Figure 3:

Flow cytometric analysis of the distribution of NK ($CD56^{+}CD3^{-}$), NK-T ($CD56^{+}CD3^{+}$), T-cells ($CD56^{-}CD3^{+}$), $CD4^{+}$ and $CD8^{+}$ antigen-experienced ($CD45RO^{+}$) T cells subsets expressing the skin homing cutaneous lymphocyte-associated antigen (CLA) in peripheral blood mononuclear cells from a healthy volunteer (upper panel) and the proband (lower panel). Note that the distribution of antigen experienced skin-homing CD4 and CD8 is preserved in the proband compared to an healthy volunteer, while the distribution of NK and NK-T is profoundly different.

Supplementary Figure 4:

A. Flow cytometric analysis of the distribution of NK ($CD56^{+}CD3$-), NK-T ($CD56^{+}CD3^{+}$), T-cells ($CD56^{-}CD3^{+}$), NK-T cells expressing the skin-homing receptor, cutaneous lymphocyte-associated antigen (CLA) or NK-T cells expressing the gut-homing chemokine receptor CCR9 in PBMCs from a healthy control (upper panel) and the proband (lower panel). Note that the expanded population of NK-T cells present in the proband's peripheral blood preferentially expresses the skin-homing receptor CLA.

B. Flow cytometric analysis of the distribution of NK-T ($CD56^{+}CD3^{+}$), T-cells ($CD56^{-}CD3^{+}$), immature NK-cells subsets ($CD3^{-}CD56^{bright}CD16^{-}$), functionally mature ($CD3^{-}CD56^{dim}CD16^{+}$) NK-cells and NK-cells expressing the skin-homing receptor CLA or the gut-homing chemokine receptor CCR9 in PBMCs from a healthy control (upper panel) and the proband (lower panel). Note that in addition to a reduced proportion of NK cells, a relative expansion of immature NK and preferential expression of the skin-homing receptor CLA is noted in the proband compared to a healthy control.

Supplementary Figure 5:

Flow cytometric analysis of the distribution of PD-1 expressing $CD4^{+}$ and $CD8^{+}$ T-cells in healthy controls (n=3) and in the proband before and 24 months after HCT.

Supplementary Figure 6:

A. Flow cytometric analysis of the distribution of Killer Ig-like Receptors (KIRs) on NK-cells of a healthy control and of the proband.

B. Flow cytometric analysis of the distribution of CD107 upon stimulation with PMA/ionomycin on NK-cells from a healthy control and the proband.

Supplementary Figure 7:

A. Flow cytometric analysis of the distribution of regulatory T-cells (Treg) in peripheral blood of a healthy control and the proband before and 24 months after HCT.

B. A representative experiment of the distribution of fluorescence intensity of phosphorylated STAT5 (pSTAT5) upon incubation with IL-2 of sorted Treg from a

healthy control (green histogram) and the proband before (blue histogram) and 24 months after HCT (red histogram).

C. Median fluorescence intensity of phosphorylated STAT5 (pSTAT5) upon incubation with IL-2 (1000 IU/mL) of sorted Treg from 2 healthy controls (green bar, 3 replicates per donor) and the proband before (blue histogram, 3 replicates) and 24 months after HCT (red histogram, 3 replicates).

Supplementary Figure 8:

Excisional inguinal lymph node biopsy of the proband collected prior to HCT: hematoxylin and eosin (left upper panel) showing architectural preservation with germinal centers and parafollicular T cell zone confirmed by immunohistochemical staining for combined CD4 (brown) and CD8 (red). Immunohistochemical staining for Foxp3 (brown) in a healthy control (right upper panel) and the proband (right lower panel) is consistent with preserved distribution of regulatory T-cells in lymphoid tissue (scale bar = 50 μm).

Supplementary Figure 9:

A. The distribution of the *IL2RG* c.191 mutated C allele in genomic DNA extracted from hematopoietic stem cells ($CD34^+$), total $CD4^+$ and $CD8^+$ T cells and maturation/differentiation CD4 and CD8 T cell subsets. The different distribution of the c.191 mutated C allele in $CD4^+$ and $CD8^+$ T cells subsets reflects the functional requirement of IL2RG signaling for maturation/differentiation.

B. The surface expression of CD132 (IL-2Rγ) in B, T and NK cells from a healthy control (upper panel) and the proband (lower panel) is presented. The V64A mutation does not affect the membrane expression of the IL-2Rγ.

Supplementary Figure 10:

A, B. The distribution of fluorescence intensity of phosphorylated STAT5 (pSTAT5) upon incubation of PBMC from a healthy control and the proband with different concentrations of IL-2 is presented. Upon gating in the $CD4^+$ and $CD8^+$ T cell subsets the black and red lines display the fold change in pSTAT5 fluorescence intensity in the healthy control or in the proband, respectively, with increasing concentrations of IL-2 (100, 1000, 5000

IU/mL) (**A**) or (**B**) IL-15 (10,100,1000 IU/mL). The fold change in median fluorescence intensity upon stimulation is presented as median and interquartile range of different independent experiments (n=5). Note that the somatic reversion of the c.191 mutated C allele results in preserved IL-2RG signaling in the $CD4^+$ and $CD8^+$ T cell subsets.

Supplementary Figure 11:

- **A.** Relative abundances of oropharyngeal microbiome, at the level of phylum. The healthy control column represents the average of samples from 2 donors. The columns for proband's pre-HCT and post-HCT represent data for 1 sample each. Note that Bacteria predominate in oropharyngeal swabs.
- **B.** From the <0.01% reads mapping to viruses, heatmap of the log transformed abundance values of the different viral species observed in the oropharyngeal samples plotted by sample.

Supplementary Figure 12:

A, B: Kinetics of donor chimerism (**A**) and absolute peripheral blood cell counts (**B**) after haploidentical hematopoietic cell transplant.

Note that full chimerism is rapidly achieved for myeloid cells, then NK cells and eventually for lymphoid cells.

Supplementary Figure 13:

Presented are $CD4^+$ (**A**) $CD8^+$-T-cell (**B**) proliferative responses to HPV16 E6 peptides, HPV16 L1 peptides and Gardasil®9 HPV 9-valent vaccine in the donor of the T-replete bone marrow graft (proband's sister immunized with Gardasil®4 in 2012), proband's before HCT (non-immunized with Gardasil®) and 24 months post-HCT (Gardasil®9 series completed on month 21 post-HCT). The proportion of CFSE negative (proliferating) T-cells is calculated for all experimental conditions after subtracting the relative experimental negative control (proportion of CFSE negative T cells with costimulatory antibodies as negative control for L1 and E6 stimulation; Adju-Phos adjuvant with costimulatory antibodies as negative control for Gardasil®9 stimulation).

Supplementary Figure 14:

Presented are $CD4^+$ (upper panels) $CD8^+$-T-cells (lower panels) intracellular cytokines production in proliferating T cells stimulated with HPV16 E6 peptides (**A**), HPV16 L1 peptides (**B**), and Gardasil®9 HPV 9-valent vaccine (**C**) in the donor of the T-replete bone marrow graft (proband's sister immunized with Gardasil®4 in 2012), proband's before HCT (non immunized with Gardasil®) and 24 months post-HCT (Gardasil®9 series completed on month 21 post-HCT). The heatmaps present the proportion of TNF$\boldsymbol{\alpha}$, IL-4 and IFN$\boldsymbol{\gamma}$ expressing cells along with the relative experimental positive (anti-CD3/CD28 beads) and negative controls (costimulatory antibodies as negative control for L1 and E6 stimulation; Adju-Phos adjuvant with costimulatory antibodies as negative control for Gardasil®9 stimulation).

Supplementary Figure 15:

A. The scatter plot in the left panel represents the fold change in the distribution of median fluorescence intensity of phosphorylated STAT5 (pSTAT5) upon incubation of sorted monocytes from 2 healthy controls and the proband before and after HCT with IL-2 (red), LPS (blue) and LPS + IL-2 (green). Each experimental condition was performed in duplicate and the median and interquartile range is plotted.

B. The scatter plot in the right panel represents the fold change in the distribution of median fluorescence intensity of phosphorylated STAT5 (pSTAT5) upon incubation of sorted monocytes from 2 healthy controls and the proband before and after HCT with IL-4. Each experimental condition was performed in duplicate and the median and interquartile range is plotted.

Supplementary Figure 16:

Heatmaps presenting the proportion of sorted monocytes from a healthy control and the proband before and after HCT expressing IL-6, IL-1$\boldsymbol{\beta}$ and TNF$\boldsymbol{\alpha}$ upon stimulation with IL-2, IL-4, LPS and LPS+ IL-2.

Supplementary Figure 17:

Depth of coverage across HPV31 (red) and HPV16 (green) genomes in samples of the hypothenar palm pre-HCT is plotted against the genomic position. The horizontal line demarcates a coverage of 5.

3. Supplementary Methods:

T-cells phenotypic analyses

Peripheral blood mononuclear cells (PBMCs) were isolated by density centrifugation. Monoclonal antibodies for the identification of T-cells, NK cells and NK-T cells extracellular and intracellular antigens were: anti-CD3-BV510 (clone OKT3, BioLegend), anti-CD4-BUV737 (clone SK3, BD), anti-CD8-BUV395 (BD), anti-CD16-BV605 (BioLegend), anti-CD56-PE-Cy7 (BioLegend), anti-Cutaneous Lymphocyte Antigen (CLA)-FITC (BioLegend), anti-CD199 (CCR9)-PE (BioLegend), anti-Perforin BV711 (BioLegend), anti-Granzyme B-Pacific Blue (BioLegend), anti-CD27-BV711 (BioLegend), anti-CD45RO-ECD (BC), anti-PD-1-BV605 (BioLegend). Dead cells were identified and excluded using the LIVE/DEAD fixable Near-IR Cell Stain kit (Invitrogen) while lymphocytes were identified according to their light-scattering properties. Flow-cytometry was performed on LSR-Fortessa (BD-Biosciences), with data analyses performed using FlowJo software (FlowJo LLC).

NK phenotypic analyses

PBMCs were isolated by density centrifugation from the proband (pre- and post-HCT), an unaffected female carrier, and 3 unrelated healthy donor controls. Extracellular immunostaining was performed with the following antibodies: CD3 (Brilliant Violet 711, clone SK7, Biolegend, 1:200), CD56 (Brilliant Violet 605, clone HCD56, 1:200), CD8a (Brilliant Violet 785, clone RPA-T8, Biolegend, 1:100), KLRG1 (APC Cy7, clone 2F1, Biolegend, 1:50), CD28 (PE, clone CD28.2, BD Biosciences, 1:50), CD27 (PE Cy5, clone O323m Thermo, 1:50), CD45RA (BUV737, clone HI100, BD Biosciences, 1:100), CD45RO (Brilliant Violet 421, clone UCHL1, Biolegend, 1:100), and CD4 (PercP Cy5.5, clone OKT4, Biolegend, 1:100). Following

extracellular staining, cells were fixed and permeabilized (Cytofix/Cytoperm, BD Biosciences) then immunostained with antibodies to perforin (FITC, clone dG9, BD Biosciences, 1:50) and granzyme B (PE-Texas Red, clone GB11, Thermo, 1:50). Data were acquired on a BD Fortessa and exported to FlowJo 10.0 for analysis (BD Biosciences). NK cells were defined as $CD56^{+}CD3^{-}$ and NKT cells as $CD56^{+}CD3^{+}$.

NK functional assays:

NK cell cytotoxicity assays were performed using PBMCs isolated by Ficoll-Paque density centrifugation. K562 target cells were incubated with 100 µCi ^{51}Cr then PBMC and target cells were co-incubated for 4 hours in a 96-well round-bottomed plate in the presence or absence of 1000 U/ml IL-2 (Roche). Following incubation, cells were centrifuged in plates and supernatant was transferred to a LUMA plate (Perkin Elmer) and dried overnight. Plates were read with a TopCount NXT and % specific lysis was calculated as follows: (sample – average spontaneous release) / (average total release – average spontaneous release) x 100. Maximal release values were generated by lysis of target cells with 1% vol/vol IGEPAL (Sigma-Aldrich).

***IL2RG* sequencing:**

Genomic DNA was isolated from PBMCs isolated by Ficoll-Paque density centrifugation using Gentra PureGene Cell kit (Qiagen). *IL2RG* exons 1-3 were amplified using Platinum Taq DNA Polymerase High Fidelity SuperMix (Invitrogen) and custom primers (813F 5'-CCAGGATCTAGGTGGGCTGAGGATTTTTGAGTCT-3' and 2276R 5'-GTAGTGCCCCTAATACCTCCTCCCTTCCCATCA-3'). FACS sorted lymphocyte subsets were lysed using RLT buffer (Qiagen), RNA isolation was performed using NucleoSpin RNA kit

(Machery-Nagel) and full-length IL2RG cDNA was produced using SuperScript IV OneStep RT-PCR kit (Invitrogen) and custom primers (2F 5'-GAGGAAACGTGTGGGTGGGGAGGGGTAGTGG-3' and 1367R 5'-CAAGTGGGGAATGCCAAATGAAGGGGTGCTTACAT-3'). PCR products were verified using agarose gel electrophoresis, residual primers were removed using ExoSAP-IT (Applied Biosystems), sequenced using Big Dye Terminators v3.1 (Applied Biosystems) and custom primers (Genomic 1450F 5'- TGGCCTCTAGTGATCCTCCTGCCTCAGCCTTTCA-3', 2276R 5'- GTAGTGCCCCTAATACCTCCTCCCTTCCCATCA-3'; cDNA 35F 5'-GAGGGACCCAGGTTCCTGACACAGACAGACTACAC-3' and 562R 5'-GGAGCCCAGGGGATCACCAGATTCTGCAGTTTTAG-3'). Residual dye terminators were removed using Performa DTR (Edge Biosystems), resulting product was run on ABI 3730 (Applied Biosystems). Chromatograms were analyzed using Sequencher (Gene Codes).

IL-2 and IL-15 stimulation assay:

PBMCs were either untreated or stimulated with different concentration of IL-2 (100, 1000, 5000 IU/mL), or IL-15 (10, 100, 1000 IU/mL) (Cell Signaling Technology) for 20 minutes at 37^{o}C in duplicate or triplicate for each experimental condition. Surface antibodies (anti-CD3-BV711, anti-CD4-BV605, anti-CD8-APC, and anti-CD56-BV421) were added and cells were fixed and permeabilized with BD Phosflow™ Perm Buffer III before adding anti-pSTAT5-Alexa Fluor 488 antibody (clone pY694, BD).

Microbiome analysis:

Sample collection, DNA isolation, library preparation, and taxonomic classification of shotgun metagenomic sequence data were performed as previously described[1]. Briefly, 37 samples were collected on one occasion from each of 2 healthy volunteers while the proband was sampled twice, once pre- and once post-transplant. Samples were collected from up to 10 skin sites representing diverse physiological characteristics: moist [antecubital crease (Ac), inguinal crease (Ic), popliteal crease (Pc), plantar heel (Ph), toe web (Tw)], dry [hypothenar palm (Hp), volar forearm (Vf)], sebaceous [manubrium (Mb), external auditory canal (Ea), and retroauricular crease (Ra)], generating ~473 million non-human, quality-filtered paired end reads (median 8,422,863 million reads per sample; minimum 381,987; maximum 43,862,854). Oropharyngeal swabs were also collected from 2 healthy volunteers and the proband pre- and post-HCT. High quality reads that did not match human hg19 human reference were mapped against a previously described database of 2349 bacterial, 389 fungal, 4695 viral and 67 archaeal reference genomes using Bowtie2's (version 2.3.2). Read hit counts were normalized by genome size. Analysis of the sequence x species matrix was performed in R version 4.0.2.

To evaluate genome coverage of high-risk HPVs, we rescreened the data using the tool HPViewer (https://github.com/yuhanH/HPViewer)[2], which maps reads to masked genomes, via bowtie. Regions of high homology between HPV strains were masked by HPViewer to reduce the likelihood of off-target read mapping. Based on this screen, we next used bwa-mem (bwa version 0.7.17) and samtools (version 1.11) coverage to determine coverage estimates for the HPV16 and HPV31 genomes from the PaVE database v1.1.

RNA Seq-based HPV genotyping of nasal SCCis

FFPE sections were removed from slides using a clean razor blade and pooled per sample (2014 and 2016 tumors). Samples were simultaneously deparaffinized and digested using 200 µL molecular grade mineral oil (Millipore-Sigma) and 127.5 µL Buffer ATL (Qiagen) with 22.5 µL of proteinase K (Qiagen). Samples were incubated overnight at 65°C in a shaking heat block. Samples were spun at max speed in a tabletop centrifuge for one minute to separate the organic and aqueous phases. Samples were subjected to an additional two-hour long digest by the addition of 12.5 µL of fresh proteinase K. 150 µL of the lysate was moved to a new tube. 250 µL of buffer PKD (Qiagen) was added and vortexed to mix. The remainder of the RNA extraction process was carried out using an RNeasy FFPE Kit (Qiagen) according to the manufacturer's protocol. RNA quantity and quality were assessed by spectrophotometry (DeNovix) and TapeStation (Agilent). Ribosomal sequence-depleted cDNA libraries were prepared using 50 ng of total RNA using the SMARTer Stranded Total RNA-Seq Kit v2 – Pico Input Mammalian (Takara) following the manufacturer instructions for FFPE tissues. Final RNA libraries were assessed for size and quantity by Agilent TapeStation. RNA libraries were sequenced on the Illumina NextSeq 550 in 2x75bp mid output mode at the CCR Genomics Core. Reads were trimmed using Trim Galore 0.6.0 with default settings. RNAseq reads were initially aligned to a fusion reference human genome containing hg38, all human viruses represented in RefSeq (as of 2018), all papillomavirus genomes from PaVE (as of 2018), https://pave.niaid.nih.gov, using STAR aligner 2.5.3ab[3]. Counts and coverage of viral reads were determined using Picard (https://broadinstitute.github.io/picard/) and bedtools (https://bedtools.readthedocs.io/en/latest/) and plotted using the R package ggplot2.

IL-2 receptor crystal structure

The crystal structure of the heterotrimeric IL-2 receptor in complex with IL-2 (accession code: 2ERJ)[4] was downloaded from the protein data bank (PDB)[5] and visualized using PyMOL[6].

Evaluation of HPV specific T-cell responses

T-cell proliferation and intracellular cytokine production was investigated by flow-cytometry upon stimulation with PepTivator HPV16 E6 peptide-pool (Miltenyi Biotec), PepMix HPV16 L1 peptide-pool (JPT), Gardasil®9 HPV 9-valent vaccine [purified virus-like particles VLPs) of the major capsid (L1) protein of HPV types 6, 11, 16, 18, 31, 33, 45, 52, 68], or/and costimulatory antibodies (αCD28, αCD49d, BD-Biosciences). Briefly, cryopreserved PBMCs were thawed and resuspended in complete RPMI media (RPMI 1640 supplemented with 10% human AB serum, 50 µg/ml Gentamicin, and 1.7 mM L-glutamine), and rested for 2 hours at 37°C in the presence of 125U/mL benzonase (Sigma-Aldrich). Cells were labeled with 10µM CFSE for evaluation of cellular proliferation and plated as 1.5 x 10^6 cells/well in 96-well deep well plate prior to stimulation with Gardasil®9 (1:50 dilution), PepMix HPV16 L1 peptide-pool (1µg/mL), or PepTivator HPV16 E6 peptide-pool (0.5µg/mL) together with costimulatory antibodies (αCD28 and αCD49d; 1 µg/ml). Cells treated with costimulatory antibodies alone (unstimulated) or Adju-Phos adjuvant (InvivoGen) together with costimulatory antibodies served as negative controls. As a positive control, cells were stimulated with Dynabeads Human T-Activator CD3/CD28 (Thermo Fisher Scientific). After cultured for 5 days, cells were transferred to a round bottom 96-well plate and re-stimulated with Gardasil®9 HPV 9-valent vaccine (1:10 dilution), PepMix HPV16 L1 peptide-pool (5µg/mL), or PepTivator HPV16 E6 peptide-pool (2.5µg/mL) together with costimulatory antibodies (αCD28 and αCD49d; 1 µg/ml). 2 hours after stimulation, brefeldin-A (50µg/mL final concentration; Sigma-Aldrich) and monensin (0.7 µg/ml final

concentration; BD-Biosciences) were added to block cytokine secretion. Cells were stimulated for 6 hours at 37°C in 5% CO_2, and then stained following the flow cytometry assay described above for IL-4, IFNγ and TNFα.

Sorting and IL-2 and IL-4 stimulation of monocytes

Briefly, cryopreserved PBMCs were thawed and resuspended in complete RPMI media (RPMI 1640 supplemented with 10% human AB serum, 50 µg/ml Gentamicin, and 1.7 mM L-glutamine), and rested for 2 hours at 37°C in the presence of 125U/mL benzonase (Sigma-Aldrich). Monocytes were sorted by using EasySep™ Human Monocyte Enrichment Kit without CD16 Depletion (Stemcell technologies). Cells were counted and adjusted to 2.5×10^5 cells/well in 96-well plate. The following stimuli were used: IL-2 (1000 IU/mL; Pepro Tech Inc); IL-4 (10 ng/mL; R&D Systems); LPS (0.5 µg/mL; Sigma). For cytokine production, 2 hours after stimulation, brefeldin-A (50µg/mL final concentration; Sigma-Aldrich) and monensin (0.7 µg/ml final concentration; BD Biosciences) were added to block cytokine secretion. Cells were stimulated for 6 hours at 37°C in 5% CO_2, and then stained following the flow cytometry assay described above. To test the signaling of IL-2 and IL-4, the phosphorylation of STAT5 or STAT6 was measured in response to stimulation with IL-2 or IL-4 respectively. Cells were either untreated or stimulated with stimuli described above for 20 minutes at 37°C. A cocktail of extracellular antibodies (anti-CD14-BV605 (BioLegend) and anti-CD16-PE-Cy7 (BioLegend)) was added to each well simultaneously. After stimulation and staining, cells were fixed with prewarmed BD Cytofix™ Fixation Buffer and permeabilized with BD Phosflow™ Perm Buffer III before adding Alexa Fluor 488-conjugated anti-pSTAT5 antibody (clone pY694; BD) or

Alexa Fluor 488-conjugated anti-pSTAT6 antibody (clone pY641; BioLegend). Samples were immediately analyzed on a Fortessa flow-cytometer (BD Biosciences).

Phenotyping, IL-2 stimulation and sorting of regulatory T-cells (Treg)

Immunophenotyping of Treg from PBMC was performed with staining of extracellular and intracellular antigens with anti-CD3-BUV395 (BD), anti-CD4-BUV737(BD), anti-CD8-PerCP-Cy5.5 (BD), anti-CD25-APC (BD), anti-CD127-BV711(BioLegend), anti-CD56-V450 (BD), and anti-Foxp3-PE (eBioscience).

To test the functionality of IL-2 receptor, an assay measuring phosphorylation of STAT5 in response to stimulation with IL-2 was used as described. Briefly, cryopreserved PBMCs were thawed, washed and rested for 2 hours at 37^{o}C. 1×10^{6} cells were seeded to each well in 96-well plate. Cells were either untreated or stimulated with IL-2 (10^{3} U/mL; Pepro Tech Inc) for 20 minutes at 37^{o}C. A cocktail of extracellular antibodies (anti-CD3-BUV395, anti-CD4-BV605, anti-CD25-APC, and anti-CD127-BV711) was added to each well simultaneously. After stimulation/staining, cells were fixed with prewarmed BD Cytofix™ Fixation Buffer and permeabilized with BD Phosflow™ Perm Buffer III before adding Alexa Fluor 488-conjugated anti-pSTAT5 antibody (clone pY694; BD). Samples were immediately analyzed on a Fortessa flow-cytometer (BD Biosciences).

Treg were sorted by using EasySep™ Human $CD4^{+}CD127^{low}CD25^{+}$ Regulatory T Cell Isolation Kit (Stemcell technologies) and used for DNA extraction and molecular analysis to determine the presence of the wild-type or V64A IL2RG allele as described above.

Hematopoietic cell transplantion platform

A fresh unmanipulated T-cell replete bone marrow graft was collected from the proband`s sister who was human-leukocyte-antigen fully matched, matched for viral serologies (EBV+, CMV-) and for blood group (O+). A reduced-intensity conditioning regimen of pentostatin, absolute lymphocyte count-targeted oral cyclophosphamide, pharmacokinetically-dosed busulfan was used. A graft dose of 4.62 x 10^8 total nucleated cells per Kg recipient ideal body weight, $CD34^+$ 4.2 x 10^6 cells per Kg, $CD3^+$ 2.63 x 10^7 cells per Kg was given. Grafy versus host disease prophylaxis was provided with high-dose, post-transplantation cyclophosphamide on days +3 and +4, mycophenolate mofetil (on days +5 through +35) and sirolimus (on days +5 through +180). The donor chimerism outcomes on day +180 were: $CD3^+$ 99%; myeloid 100%, NK 96%; day 720: $CD3^+$ 100%; myeloid 100%, NK 100% (**Suppl. Fig.12**).

4. Supplementary Table

	Proband Pre-HSC	Proband^ Post-HSC	Matched-related donor (sister)	Normal range
Lymphocyte subsets count (cells/μL)				
Total $CD3^+$ T cells	3323	895	1673	675-2235
$CD4^+$ T cells	287	406	960	359-1565
$CD8^+$ T cells	2907	476	695	178-853
B cells	295	282	202	50-329
NK Cells	181	252	137	126-729
NK-T Cells	2880	16	na	29-299
Immunoglobulin (mg/dL)				
IgG	1835	1363	1054	700-1600
IgA	357	287	143	70-400
IgM	106	62	114	40-230
IgD	3	5	3	< 10
IgE (IU/mL)	<1	130	153	0-90
Anti-CMV IgG and IgM	Negative	na	Negative	
Anti-HSV1 IgG	Negative	na	Positive	
Anti-HSV2 IgG	Positive	na	Negative	
Anti-Varicella Zoster Virus IgG	Negative	na	Positive	
Epstein-Barr virus capsid antigen IgG	Positive	na	Positive	
Epstein-Barr virus capsid antigen IgM	Negative	na	Negative	
Epstein-Barr virus nuclear antigen	Positive	na	Positive	
Anti-Toxoplasma IgG (IU/mL)	< 0.2	< 0.2	< 0.2	
Anti-Diphtheria (IU/mL)	Positive (0.02)	>1.00*	na	
Anti-Tetanus (IU/mL)	Positive (0.16)	1.66*	na	

^ 24 months post-HCT; *Post-immunization**;** na: not available.

5. Supplementary Methods References:

1. Tirosh O, Conlan S, Deming C, et al. Expanded skin virome in DOCK8-deficient patients. Nat Med 2018; 24: 1815-21.

2. Hao Y, Yang L, Galvao Neto A, et al. HPViewer: sensitive and specific genotyping of human papillomavirus in metagenomic DNA. Bioinformatics 2018;34:1986-95.

3. Dobin A., Davis C.A., Schlesinger F., Drenkow J., Zaleski C., Jha S., Batut P., Chaisson M., Gingeras T.R. STAR: ultrafast universal RNA-seq aligner. Bioinformatics 2013; 29: 15-21.

4. Stauber DJ, Debler EW, Horton PA, Smith KA, Wilson IA. Crystal structure of the IL-2 signaling complex: paradigm for a heterotrimeric cytokine receptor. Proc Natl Acad Sci U S A. 2006; 103: 2788-93.

5. Goodsell DS, Zardecki C, Di Costanzo L, Duarte JM, Hudson BP, Persikova I, Segura J, Shao C, Voigt M, Westbrook JD, Young JY, Burley SK. RCSB Protein Data Bank: Enabling biomedical research and drug discovery. Protein Sci. 2020; 29: 52-65.

6. https://pymol.org/